Pergamon

Int. J. Multiphase Flow Vol. 24, No. 3, pp. 411–430, 1998

Printed in Great Britain
PII: S0301-9322(97)00068-2
0301-9322/98 $19.00 + 0.00

FLUID DISPLACEMENT BY HIGH REYNOLDS NUMBER BUBBLE MOTION IN A THIN GAP

J. W. M. BUSH and I. EAMES

Department of Applied Mathematics and Theoretical Physics, University of Cambridge, Silver Street, Cambridge, CB3 9EW, U.K.

(Received 11 October 1996; accepted 14 August 1997)

Abstract—The fluid displacement associated with the injection and subsequent translation of high Reynolds number bubbles in a thin gap is examined experimentally, and compared with a theoretical model based on a two-dimensional inviscid flow calculation. In the experiments, air bubbles are injected and rise through an aqueous solution bound in a thin gap. Particular attention is given to the parameter regime characterised by the steady rectilinear motion of oblate elliptical or elliptical cap bubbles which transport a closed volume of fluid which trails the bubble in the form of a stable primary wake, and by laminar flow in the suspending fluid. The fluid displacement is measured by digitally tracking either particles suspended in the fluid, or the distortion of an initially horizontal fluid–fluid interface. While the fluid transport associated with the narrow region of viscous influence, or secondary wake, trailing the bubble is observed to contribute to the total fluid displacement over long times, its contribution is minimized by the influence of the channel walls. We thus focus on the fluid displacement associated with the irrotational component of the flow, which is described in terms of two components: a positive "drift" component which is localized near the point of crossing, and a negative "reflux" component required by continuity in a bounded domain.

The experimental observations confirm a number of theoretical predictions concerning the fluid displacement accompanying high Reynolds number bubble motion. At distances greater than half the channel width from the point of injection, both the injection-induced displacement and the reflux are spread uniformly across the channel width. The reflux amplitude depends on the size of the primary wake, the drift volume and the channel width. The drift volume does not depend on the detailed shape of the bubble and wake or on the channel width, but is uniquely set by the cross-sectional area of the compound body composed of bubble plus wake. The shape of a distorted material surface depends weakly on the compound body shape, and becomes more peaked as the compound body becomes more oblate. This indicates that the presence of a primary wake adjoining a bubble will influence the longitudinal dispersion rather than the total drift volume.

The relevance of this study for the analogous three-dimensional problem is discussed, and a heuristic model of mixing by high Reynolds number bubbles in a bounded domain is developed. The importance of fluid transport in the secondary wake, which was neglected in the theoretical model, is discussed in detail.

Key Words: bubbles, transport, drift, reflux

1. INTRODUCTION

The transport properties of high Reynolds number bubbles are of interest in a variety of industrial and environmental applications; for example, in boiling convective flows, where vaporization near heating elements creates bubbles which may contribute significantly to the total heat flux (Mayinger *et al.* 1991); in a number of purification and aeration systems, where chemical transport across the bubble surface is important; in gas fluidised beds, where the motion of voids is remarkably similar to that of high Reynolds number bubbles with zero surface tension (Davidson and Harrison 1963); in bioreactors, where bubbling serves to aerate the suspended microorganisms and disperse toxic waste products; in the meltdown phase of nuclear reactor accidents, where bubbles are produced by the reaction between the molten reactor core and the concrete containment wall; and in the destratification of lakes and the containment of oil spills by bubble plumes (Asaeda and Imberger 1993).

A prerequisite to the study of fluid transport by an assemblage of bubbles is a thorough understanding of that associated with the motion of single bubbles. It is particularly important to be able to characterize the fluid transport in terms of the governing parameters; specifically, the form of the bounding geometry, and the properties of the bubble surface and suspending

fluid. In order to identify the various mechanisms contributing to the fluid transport, one must have a clear physical picture of the bubble-induced flow.

We are concerned with the parameter regime in which the Reynolds number, $Re = Ur/v$, based on the bubble rise speed U, the undeformed bubble radius r and the kinematic viscosity v of the suspending fluid, is sufficiently large that viscous effects are confined to thin boundary layers, but sufficiently small that the bubble motion is steady and stable, and the external flow is everywhere laminar. In this limit, the bubble shape and induced flow are uniquely prescribed by Re and the Eotvos number $\Sigma = \rho g r^2/\sigma$, which indicates the relative importance of the hydrostatic pressure and the curvature force associated with the surface tension σ in the normal stress balance. Moreover, in this limit, the flow induced by the rising bubbles is to leading order described by inviscid irrotational flow theory. However, there must also be regions of non-zero vorticity at the surface of the bubble in order to satisfy the tangential stress boundary condition at the bubble surface (zero tangential stress for the ideal case of a clean bubble). Vorticity generated at the bubble surface is advected downstream, giving rise to a secondary wake which spreads downstream and contributes to a fluid transport towards the bubble. Far downstream of a bubble rising in unbounded flow, the vertical volume flux Q in the secondary wake is related to the hydrodynamic drag D on the bubble through

$$D = \rho U Q \qquad [1]$$

(Batchelor 1967). While the flow upstream of the bubble may be adequately described as inviscid (Davies and Taylor, 1950), the details of the wake region downstream of the bubble depend explicitly on the boundary layer structure adjoining the bubble.

Moore (1965) considered the motion of small nearly spherical bubbles ($\Sigma \ll 1$), and developed a theoretical model describing the viscous boundary layers on the bubble surface (treated as free-slip) and in a thin vortical filament trailing the bubble corresponding to the secondary wake. Moore's predictions for the bubble shapes and hydrodynamic drag values have been confirmed by recent experimental studies of millimetre scale air bubbles rising through hyperclean water (Duineveld 1995; see also Maxworthy *et al.* 1996). Ryskin and Leal (1984) calculated the flow around deformed bubbles at moderate Σ, and demonstrated the presence of closed vortical regions, or "primary wakes", adjoining the trailing edge of the bubble at sufficiently large Σ. At higher Reynolds numbers, the instability of the primary wake causes a path instability resulting in a zigzag or helical bubble trajectory (Saffman 1956; Hartunian and Sears 1957). At still higher Reynolds and Eotvos numbers, the bubble assumes a spherical cap shape whose wake is ultimately turbulent and path unsteady. Maxworthy (1967) examined the unsteady motion of a spherical cap air bubble through water, and argued that the turbulent wake trailing the bubble was open.

A number of experiments have been performed in order to examine high Re bubble motion in a two-dimensional geometry, and have involved the motion of air bubbles through water bound in a thin gap. The evolution of the bubble shapes and flow structure with increasing bubble volume is roughly analogous to the three-dimensional case, and has been detailed by Siekmann *et al.* (1974). Lazarek and Littman (1974) measured the pressure field around circular cap bubbles rising in a narrow channel, and demonstrated that the flow downstream of the bubble is consistent with Collins' (Collins 1965a) qualitative observations of a vortex pair trailing the bubble in a stable primary wake, and, moreover, that the flow upstream of the bubble is well approximated by the irrotational flow around the oval compound body composed of bubble plus primary wake. Bessler and Littman (1987) demonstrated that even in the case of a fully turbulent wake, there is a closed volume of fluid or primary wake trailing a circular cap bubble.

We thus identify three distinct mechanisms of fluid transport associated with bubble motion at high Re. Firstly, there may be transport of a closed volume of fluid corresponding to the primary wake. Secondly, there is the fluid displacement associated with the potential flow around the compound body. Thirdly, there is the transport contributed by the secondary wake. In this paper, we present the results of an experimental study of bubble motion in a thin gap in which we focus on the parameter regime characterised by the steady rectilinear motion of bubbles with stable attached primary wakes and a laminar external flow, and attempt to quantify the relative

importance of each of these three transport mechanisms. Specifically, we observe displacements associated with the injection and subsequent translation of the bubble and compare them with a theoretical description based on a two-dimensional inviscid flow model.

Darwin (1953) considered the inviscid fluid displacement associated with the translation of rigid bodies, and described the distortion of an initially horizontal material surface by the vertical translation of a body in an infinitely long vertical channel. Darwin demonstrated that the distortion could be characterized by two components: a positive displacement, or "drift", which is confined to a region close to the point of crossing; and a negative displacement, or "reflux", which is spread uniformly across the channel width (refer to figure 1). Darwin's Proposition relates the drift volume V_d to the body volume V through $V_d = C_m V$, where C_m is the added mass coefficient of the body. Continuity requires that the reflux volume be equal to the sum of the body and drift volumes, $(1 + C_m)V$. Darwin predicted that the reflux will be uniformly distributed across the channel, so that the amplitude of the reflux across a two-dimensional channel of width w is $z_r = (1 + C_m)V/w$. We note that the reflux component of the fluid displacement depends explicitly on the size of the container, while the drift component does not.

While a great deal of research has been focussed towards understanding the shapes and rise speeds of high Re bubbles (see Clift *et al.* 1978), there have been very few experimental studies of the associated fluid displacement. Weber and Bhaga (1982) considered the fluid displacement associated with three-dimensional bubbles with closed wakes ($2 < Re < 110$) rising along the axis of a cylindrical tube, and pointed out the important contribution of the secondary wake to the total fluid transport. Bataille *et al.* (1991) examined three-dimensional air bubbles of effective diameter 2.5–5.5 mm rising through an interface between two aqueous solutions. They observed that, as Re increased from 500 to 1300, the ratio of drift to bubble volumes increased from 0.5 (the value anticipated for a spherical bubble on the basis of Darwin's Proposition) to 3.0. No description of either the bubble shapes, wakes or the form of the bubble motion was provided, and no explanation for the increase in the ratio of drift to bubble volume with increasing Re was reported. However, the data compiled in Clift *et al.* (1978) indicates that in the parameter regime considered by Bataille *et al.* (1991), one expects to observe unsteady motion of oblate ellipsoidal bubbles; consequently, Darwin's description of fluid transport by steady bubble motion is not directly applicable. Finally, neither Weber and Bhaga (1982) nor Bataille *et al.*

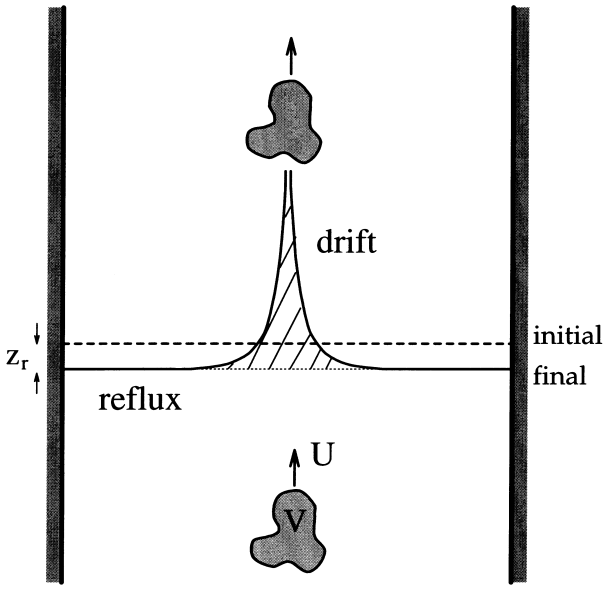

Figure 1. Darwin's model of inviscid fluid displacement by an arbitrarily shaped rigid body of volume V and added mass coefficient C_m translating in an infinite channel. The drift occurs in a thin filament drawn up behind the body, and the drift volume (shaded) is $V_d = C_m V$. The reflux volume (that between the two horizontal lines) is required by continuity to be $(1 + C_m)V$, and is spread uniformly across the channel width; consequently, the reflux amplitude in a channel of width w is given by $z_r = (1 + C_m)V/w$.

(1991) were able to measure the form of the reflux accompanying the bubble motion in their experiments, as its magnitude was too small to be measured in their three-dimensional geometry.

We present an experimental method for considering fluid displacement associated with high *Re* bubble motion, which involves tracking the distortion of an initially horizontal fluid–fluid interface by a bubble rising in a thin gap. While experimental studies of bubble motion in a thin gap of water have been used previously to verify details of the adjustment phase (Walters and Davidson 1962) and rise speeds (Collins 1965b) predicted by two-dimensional inviscid flow theory, they have yet to be used to examine the associated fluid displacement. Our experimental technique has three significant advantages over those employed in the analogous three-dimensional studies. Firstly, it is possible to accurately resolve the form and magnitude of both the drift and reflux. Secondly, flow visualization was greatly facilitated, and so we were able to readily observe details of the bubble shape and external flow. Thirdly, it was possible to incline the channel at an arbitrary angle θ relative to the horizontal, and so to adjust the effective gravity $g\sin\theta$ driving bubble motion. This flexibility made it possible to explore a broad range of parameter space and, in particular, to focus on the desired regime of laminar flow around bubbles rising steadily with stable primary wakes.

We consider the fluid displacement associated with the injection and subsequent translation of single bubbles in a bounded rectangular channel. In Section 2, we present the governing equations, and describe the parameter regime to be considered in our experimental study. A theoretical model of inviscid fluid displacement by the injection and translation of a two-dimensional bubble is presented in Section 3. While the theoretical model may be extended in order to describe the analogous three-dimensional problem, we focus here on the two-dimensional case in order to facilitate comparison with our experimental study. In Section 4, we present a detailed account of our experimental study of fluid transport by high *Re* bubbles, and compare our observations with the predictions of the inviscid flow theory. In Section 5, we apply our physical picture of fluid displacement by high *Re* bubbles in order to develop a simple model of mixing by an assemblage of bubbles in a bounded geometry. A number of results of our study are discussed in the context of fluid displacement by three-dimensional bubble motion in Section 6.

2. BUBBLE MOTION IN A THIN GAP

Consider a fluid of uniform density ρ and kinematic viscosity ν confined within a thin channel of thickness d and width w such that $d \ll w$. The bounding plates of the channel are inclined at an angle θ relative to the horizontal. We introduce a Cartesian coordinate system (x,y,z) such that x and z vary along, respectively, the width and the length of the channel, and $y = 0$ and $y = d$ define the upper and lower channel boundaries. A bubble of volume $V = \pi r^2 d$ (treated here as inviscid, zero density fluid) is injected at a distance z_o from the lower boundary. The characteristic bubble size r is large relative to the gap thickness, $r/d \gg 1$, so that flow induced within the channel is largely two-dimensional, that is, confined to lie within planes parallel to the channel walls.

As the bubble rises, it rapidly adjusts to an equilibrium shape. In the high Reynolds number limit, $Re \gg 1$, viscous stresses do not contribute appreciably to the normal stress balance at the bubble surface, and the bubble shape is uniquely prescribed by *Re* and the Eotvos number $\Sigma = \rho g r^2 \sin\theta/\sigma$ defined in terms of the effective gravity component $g\sin\theta$ aligned with the direction of motion. While a variety of bubble shapes were observed in our experimental study, we focus on the parameter regime in which the bubbles assume an oblate elliptical or elliptical cap form, and transport a volume of fluid ϵV in a stable closed primary wake (refer to figure 2). In this case, we describe the total fluid displacement as that due to the radial injection of a volume V, and the subsequent steady translation of the oval compound body of volume $(1 + \epsilon)V$ composed of bubble plus primary wake.

Nondimensionalizing the Navier–Stokes equations on the basis of a horizontal lengthscale r, convective timescale r/U, velocity scale U, cross-channel lengthscale d, and dynamic pressure scale ρU^2 yields the equations governing incompressible fluid motion in the channel:

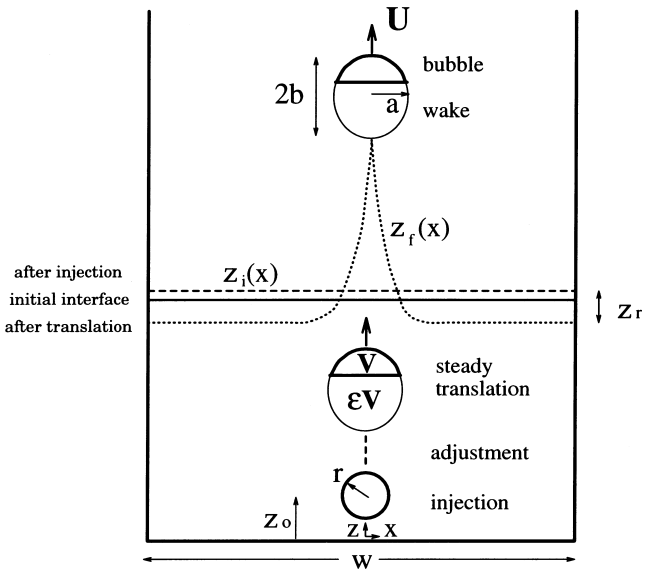

Figure 2. Theoretical model of inviscid fluid displacement by the injection and subsequent steady translation of a two-dimensional bubble with a stable wake. At time $t = 0$, a bubble of volume $V = \pi r^2$ is injected a distance z_0 from the lower boundary. After a rapid adjustment period, the bubble assumes a steady shape with a stable primary wake of volume ϵV. The total fluid displacement within the channel is that associated with the injection of a circular bubble of radius r and the subsequent translation of the elliptical compound body composed of bubble plus primary wake. Darwin's Proposition relates the drift volume to that of the compound body through the added mass coefficient of the compound body, $C_m' = a/b$.

$$\frac{D\mathbf{u}}{Dt} = -\nabla p_{\mathrm{d}} + \frac{\nu}{Ur}\left(\frac{r}{d}\right)^2 \frac{\partial^2 \mathbf{u}}{\partial y^2},\ \nabla \cdot \mathbf{u} = 0, \qquad [2]$$

where we have introduced a dynamic pressure, $p_d = p - \rho g z \sin\theta$, and employed the thin gap approximation, $(d/r)^2 \ll 1$, in order to retain only the dominant viscous term. In the limit of $Re(d/r)^2 \gg 1$, viscous effects are confined to thin boundary layers adjoining the channel walls and bubble surface, and the bulk interior may be treated as inviscid. The horizontal vorticity associated with the no-slip condition at the rigid walls does not diffuse across the gap in a convective timescale r/U:

$$\frac{\text{DIFFUSION TIME}}{\text{CONVECTIVE TIME}} = \frac{d^2/\nu}{r/U} = Re\left(\frac{d}{r}\right)^2 \gg 1. \qquad [3]$$

The flow profile within the gap corresponds closely to the flat profiles observed in pressure-driven start-up flows. As $Re(d/r)^2 \to \infty$, the bubble-induced fluid motion may thus be described to leading order as two-dimensional inviscid flow:

$$\frac{D\mathbf{u}}{Dt} = -\nabla p_{\mathrm{d}},\ \nabla \cdot \mathbf{u} = 0, \qquad [4]$$

so that the velocity field may be expressed in terms of a potential ϕ through $\mathbf{u} = \nabla\phi$. The motion of bubbles in a thin gap has been considered by Walters and Davidson (1962) in a study of the adjustment phase of a circular bubble released from rest, and by Collins (1965b) in a study of the steady translation phase of circular cap bubbles. Both investigators found that the experimental observations of the bubble motion validated simple theoretical models based on equation [4] governing two-dimensional inviscid flow.

It is possible to assess the extent to which criterion (3) is satisfied by the two components of the flow associated with the bubble injection and translation. Since the velocity field associated with the injection of a circular bubble of radius r in a time τ is given by $|\mathbf{u}| \sim r^2\tau^{-1}(x^2 + z^2)^{-1/2}$, criterion (3) is satisfied everywhere within a distance $rd^2/(\nu\tau)$ of the point of injection. Since the

velocity field associated with the steady translation at speed U of a circular body of radius r is given by $|\mathbf{u}| \sim Ur^2(x^2+z^2)^{-1}$, criterion (3) is satisfied during the translation phase everywhere within a distance $Re^{1/2}d$ of the rising bubble. To summarize, the injection- and translation-induced flow may be adequately described with two-dimensional inviscid flow theory everywhere within the bounded channel provided the channel dimension L is such that

$$L \ll \min\left(Re^{1/2}d, \frac{rd^2}{\nu\tau}\right). \quad [5]$$

In our experimental study, the injection time was sufficiently short (typically 0.01 seconds) that the fluid motion induced during the injection phase could everywhere be adequately described by inviscid flow theory. Moreover, in our experiments, typically $Re \sim 4000$, $d \sim 0.25$ cm and $r \sim 1$ cm, so that $Re^{1/2}d$ was typically 15 bubble radii, which provided an upper bound for our channel width.

It is also important to recognize that there must be a contribution to the fluid transport made by the secondary wake, which cannot be accounted for on the basis of inviscid flow theory. The irrotational flow component contributes a permanent distortion to a material surface, while the flow associated with the secondary wake will continue to distort the interface until its influence is damped out by viscous interaction with the bounding geometry. In the two-dimensional geometry of our experiments, the kinetic energy in the secondary wake will be damped by the channel walls on a timescale d^2/ν rather than spreading downstream on a diffusive timescale. Since the walls act to reduce and eventually suppress the motions in the secondary wake, we do not attempt to quantify the contribution of the secondary wake to the fluid transport, but instead focus on the contribution made by the irrotational component of the flow.

3. THEORETICAL ANALYSIS OF FLUID DISPLACEMENT

In this section we describe the distortion of an initially horizontal line of marked fluid by the injection of a circular bubble and the subsequent translation of an elliptical compound body composed of bubble plus primary wake (refer to figure 2). We consider the equations governing two-dimensional inviscid flow, namely Euler's equation [4], and so predict drift and reflux volumes consistent with the application of Darwin's Proposition to the compound body.

The total displacement in the z-direction associated with the bubble-induced flow is defined as $z = \int_{t=0}^{\infty} u_z \, \mathrm{d}t$.

3.1. *Displacement due to bubble injection*

The injected bubble is assumed to expand radially from a point a distance z_0 from the lower boundary. The associated inviscid flow is calculated by using the distribution of sources required to satisfy the kinematic boundary conditions on the channel walls. The injection-induced distortion, z_i, due to a source in a bounded geometry was calculated by Eames and Duursma (1997), who showed that far from the point of injection (*i.e.* $(z-z_0)/r \gg 1$) the final shape of the interface may be expressed in terms of distance x from the centerline as

$$z_i(x) \sim \frac{V}{w}\left(1 + \exp\left(-\frac{2\pi(z-z_0)}{w}\right)\cos\left(\frac{2\pi x}{w}\right)\right). \quad [6]$$

The injection-induced displacement decreases monotonically with distance from the centerline, and is constant to within 5% provided $(z-z_0)/w > 0.5$, that is, at distances greater than half the channel width from the point of injection.

3.2. *Displacement due to bubble translation*

We assume that, following injection, the bubble undergoes a rapid adjustment to a form whose elliptical compound body, composed of a bubble of volume V plus a primary wake of volume ϵV, may be described as an ellipse with a half-width a, and half-length b (refer to figure 2).

The distortion of the marked surface is calculated as the bubble moves from a distance $z - z_0$ below the marked surface, to a distance infinitely far above it. Eames *et al.* (1994) showed that the displacement of a marked fluid parcel by the potential velocity field $\mathbf{u} = (u_x,u_z) = \nabla\phi$ is in general given by

$$z_f(x) = \int_0^\infty u_z \mathrm{d}t = z_r + z_d = \underbrace{-\left[\frac{\phi}{U}\right]_{(x,-\infty)}^{(x,z-z_0)}}_{\textbf{reflux}} + \underbrace{\int_0^\infty \frac{u_x^2 + u_z^2}{U}\,\mathrm{d}t}_{\textbf{drift}}, \qquad [7]$$

The first term in equation [7], z_r, corresponds to the negative displacement associated with reflux. When the elliptical bubble is initially far from the marked surface, *i.e.* $(z - z_0)/a \gg 1$, the reflux may be expressed as (Eames *et al.* 1994)

$$z_\mathrm{r}(x,z) \sim -\frac{\pi a(a+b)}{w}\left(1 + 2\exp\left(-\frac{2\pi(z-z_0)}{w}\right)\cos\left(\frac{2\pi x}{w}\right)\right). \qquad [8]$$

Reflux is critically dependent on both the initial separation of body and interface, and the channel width w. The kinematic effect of the walls is significant even when the channel is very wide: as $w \to \infty$, the reflux amplitude tends to zero, but the reflux volume remains finite. The reflux amplitude is constant to within 5% and effectively independent of the initial separation of body and marked interface when $(z - z_0)/w > 0.6$, which indicates that the characteristic time-scale over which reflux contributes to the total fluid displacement is U/w. In the limit of $(z - z_0)/w \to \infty$, corresponding to the case of a bubble approaching from -∞, [8] yields Darwin's result of uniform reflux across the channel width.

The second term in equation [7], z_d, corresponds to the positive displacement, associated with fluid drift. In order to calculate the drift component of the fluid displacement associated with a translating ellipse, we use the velocity potential given by Batchelor (1967):

$$\phi(x,z) = U\left(\eta + \frac{c^2}{\eta}\right)\sin\zeta - U_x, \qquad [9]$$

where the elliptical coordinates (η,ζ) are defined through

$$z(\eta,\zeta) = \eta\left(1 + \frac{\lambda^2}{\eta^2}\right)\cos\zeta,\ x(\eta,\zeta) = \eta\left(1 - \frac{\lambda^2}{\eta^2}\right)\sin\zeta, \qquad [10]$$

and the geometrical coefficients are

$$c = \frac{1}{2}(a+b),\ \lambda = \frac{1}{2}(a^2 - b^2)^{1/2}. \qquad [11]$$

The drift component of the fluid displacement associated with a translating ellipse may thus be described by the asymptotic expressions

$$z_\mathrm{d}(x) \sim \begin{cases} \dfrac{\pi a^2(a+b)^2}{8x^3}, & x \gg a, \\ \dfrac{2a^2}{a+b}\log\left(\dfrac{(4(a+b)}{x}\right), & x \ll a. \end{cases} \qquad [12]$$

The drift displacement is localized near the point of crossing (with amplitude z_d decaying rapidly as $1/x^3$ far from the point of crossing), and has a logarithmic singularity at the point of crossing $x = 0$. The drift amplitude depends only very weakly on the geometric details of the bounding container. In particular, the finite initial separation of bubble and interface, $(z - z_0)$, and the finite width of the container w typically alter the drift amplitude by amounts of $O(a^2/(z - z_0))$ and $O(a^3/w^2)$, respectively, relative to that in an unbounded system (Eames *et al.* 1994).

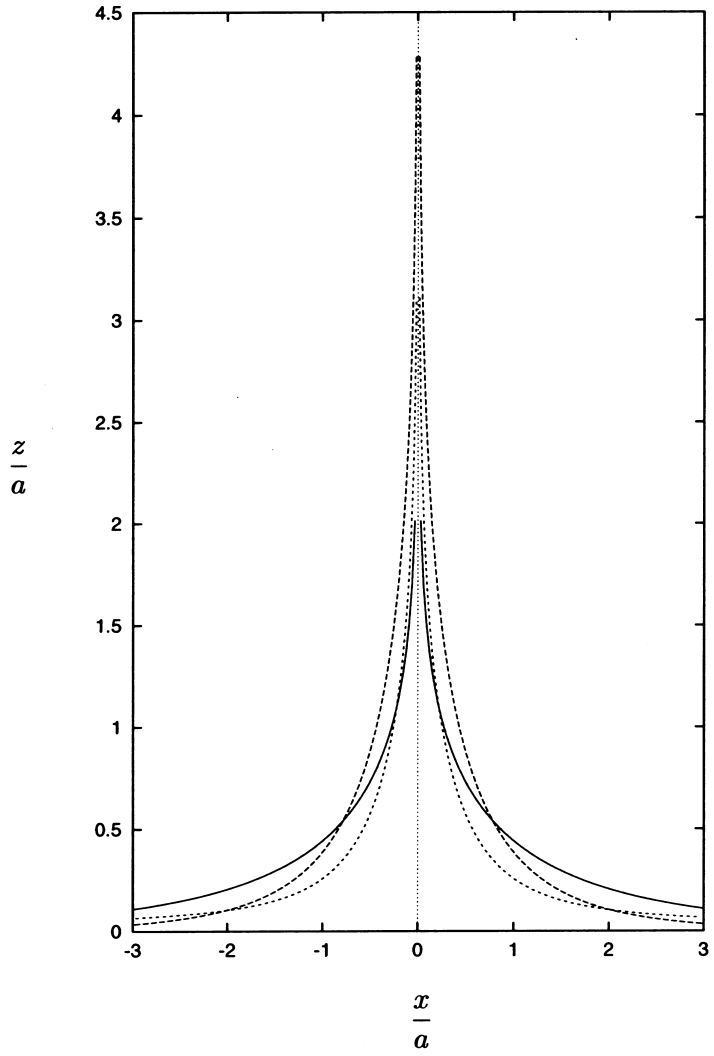

Figure 3. The drift component of the distortion of an initially horizontal material surface by translating two-dimensional elliptical bodies. The cross-sectional area $2a$ of the bodies is identical, while the width to height ratio, a/b, assumes the values 0.3 (solid line), 1.0 (dotted line) and 3.0 (dashed line).

Thus when $a^2/w^2 \ll 1$ and $a/(z - z_0) \ll 1$, the contribution of drift to the fluid displacement may be calculated to leading order by considering the deformation of a material surface in an unbounded system.

Figure 3 illustrates the distortion profiles associated with translating elliptical bodies with identical cross-sectional widths but different lengths. The displacement associated with fluid drift is clearly localised, and occurs over a distance characterised by the body width. Note that while the drift volumes are equal for each case, the final interface shapes are different. In particular, the peaks are more and less pronounced, respectively, for oblate ($a/b > 1$) and prolate ($a/b < 1$) elliptical bodies.

In general the fluid drift is localised and independent of the details of the bounding geometry. Conversely, the reflux is broadly distributed across the channel width, and has a form which depends explicitly on both the channel width and the initial distance between the bubble and interface, $z - z_0$. For the sake of comparison with our experimental study, we calculate the deformation of a material surface by first calculating the deformation of the material surface in unbounded flow, which gives the drift contribution, then subtracting the appropriate constant reflux amplitude.

Finally, it is worth noting that the fluid displacement associated with the inviscid component of the flow occurs much more rapidly than that associated with the transport in the secondary wake. In particular, the components of fluid displacement associated with drift and reflux occur over characteristic timescales of, respectively, a/U and w/U. Conversely, in the absence of viscous interaction with the bounding geometry, the secondary wake will give rise to a constant volume flux towards the bubble in the far field.

3.3. *Drift and reflux volumes*

If the channel were vertically unbounded, and the bubble approaching from -∞, Darwin's Proposition would indicate that the ratio of the drift volume, V_d, to the compound body volume, $(1 + \epsilon)V$ is given by the added mass coefficient of the compound body, $C_m' = a/b$. In this case, the drift volume is given by

$$V_{\mathrm{d}} = \int_{-w/2}^{w/2} z_{\mathrm{d}} dx = C_{\mathrm{m}}' V' = \frac{a}{b}(1+\epsilon)V = \pi a^2. \qquad [13]$$

Consequently, the drift volume, $V_d = \pi a^2$, depends to leading order neither on the channel width nor on the detailed shape of the compound body, but only on the cross-sectional area of the compound body presented to the flow.

The total fluid, V_t, transported by the bubble across a given material surface is given by the sum of the primary wake, V_p, and drift volumes:

$$V_{\mathrm{t}} = V_{\mathrm{p}} + V_{\mathrm{d}} = C_{\mathrm{m}}'(1+\epsilon)V + \epsilon V. \qquad [14]$$

The fact that V_t is generally significantly greater than the bubble volume V indicates that the high Re motion of bubbles with wakes may be an extremely efficient fluid transport mechanism. For example, $V_t = 7.6V$ in the special case of a two-dimensional circular cap bubble ($C_{\mathrm{m}}' = 1$, $\epsilon = 3.3$).

The reflux volume, necessitated by global continuity, must be equal to the sum of the bubble, primary wake and drift volumes:

$$V_{\mathrm{r}} = \int_{-w/2}^{w/2} z_{\mathrm{r}} dx = -(1 + C_{\mathrm{m}}')(1+\epsilon)V. \qquad [15]$$

Equation [8] indicates that, at sufficient distances from the lower boundary, the reflux will be uniformly distributed across the channel width; consequently, the reflux amplitude is given by

$$z_{\mathrm{r}} = -\frac{(1 + C_{\mathrm{m}}')(1+\epsilon)V}{w}, \qquad [16]$$

which again depends explicitly on the channel width w.

3.4. *Fluid trajectories*

The trajectory of a fluid parcel initially located at a point ($x(0)$, $z(0)$) is calculated by integrating the disturbance velocity associated with the translating elliptical body:

$$\mathbf{x}(t) = (x(t), z(t)) = (x(0), z(0)) + \left(\int_0^t u_{\mathrm{x}} dt, \int_0^t u_z dt \right). \qquad [17]$$

The trajectory of a fluid parcel depends on its initial position ($x(0)$, $z(0)$). For the case of a bubble approaching from infinitely far away, $z(0) - z_0 \to \infty$, all particle trajectories must be fore–aft symmetric, and no net horizontal displacement may occur (refer to figure 8). A fluid parcel near the point of crossing, $x(0) < a$, will be pushed ahead of the approaching-bubble, then swept around the bubble and into the downstream region, thus being displaced substantially in a horizontal direction and suffering a large net vertical displacement (corresponding to drift). The final trajectory thus assumes a looping form. The amount of horizontal displacement decreases as $x(0)$ increases. A fluid parcel initially far from the point of crossing, $x(0) \gg a$, suffers a net

negative vertical displacement (corresponding to reflux), and executes a curved trajectory whose curvature decreases with increasing $x(0)$.

4. EXPERIMENTS

Figure 4 is a schematic diagram of the experimental apparatus. Two 12 mm thick glass plates were clamped together, and separated at their edges by a 2.5 mm thick margin of rubber spacer. The channel width w was varied by adjusting the horizontal placement of the side-wall spacers. The channel was mounted on a frame, and could be oriented at an arbitrary angle θ relative to the horizontal. Air bubbles were introduced manually with a syringe at the base of the channel. The bubble-induced fluid motion was visualized by one of two techniques, either particle tracking of a homogeneous suspending fluid, or digital tracking of the interface between two distinct fluids of comparable density.

4.1. *Experimental method*

In order to resolve the flow field through particle tracking, the channel was filled with a dilute saltwater solution seeded with neutrally buoyant white plyolite particles (of diameter 200–300 μm and density 1033 kg/m^3), which were clearly visible against the lower plate of black glass. The flow induced by the bubble motion was recorded on video, and the particle trajectories were deduced using the DigImage image processing system (Dalziel 1992). While the particle tracking adequately resolved the reflux associated with the bubble motion, the rapid motions in the primary wake and those associated with the drift of material forward were not as readily resolved. Consequently, interface tracking rather than particle tracking was used in order to calculate drift volumes.

The second method employed for observing the distortion of a material surface was to set up a fluid–fluid interface stabilized by a small density difference. For this purpose, the upper fluid was pure distilled water, while the lower was a dilute milk–water solution (20% milk, $\rho = 1.003$ g/cc). Over the timescale of the experiments, typically two seconds, both diffusion of the milk–water interface and convection associated with the small density difference of the two fluids were negligible, so that the interface behaved like a material surface. Moreover, the pre-

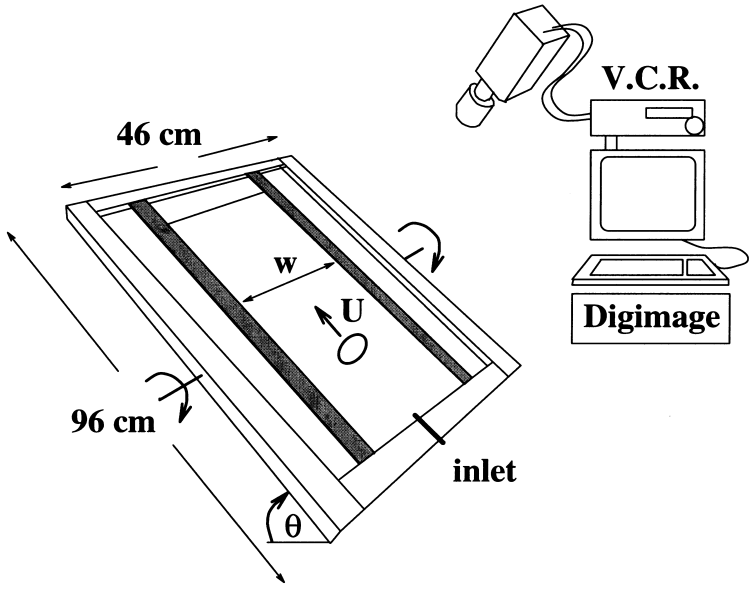

Figure 4. A schematic illustration of the apparatus used in the experimental study. Air bubbles were injected into a thin (2.5 mm) layer of aqueous solution bound between glass plates. The channel could pivot about a horizontal axis, and so be oriented at an arbitrary angle θ relative to the horizontal.

sence of surfactants in the milk did not bring about an appreciable change in shape as the bubble passed through the interface.

Images of the interface were captured before injection, after injection, and after the bubble had passed through the interface a distance comparable to the channel width. By this time, the contribution to the fluid displacement by the potential flow is complete, and the subsequent weak distortion is that associated with the secondary wake. The form of the distortion of the interface associated with the injection and translation phases could be observed by superposing the three images. The images captured after injection and translation were superposed, and the volumes associated with the bubble, the primary wake, the drift and the reflux were colour coded (refer to figure 5) and calculated digitally by pixel-counting. As a check on the accuracy, we computed the ratio of the volumes displaced forward $C + D + E$ and backward A. Any violation of continuity indicated that turbulence was mixing the milkwater solution with the water, thereby bringing about an apparent increase in the volume of the milkwater solution.

The advantage of interface tracking over particle tracking was the ease with which the primary wake and drift profiles were resolved. It was also straightforward to discern when turbulence was present in the wake of the bubble. When turbulence was observed in the wake, not only was the continuity of milk solution apparently violated by mixing processes, but it was virtually impossible to distinguish between the primary wake and drift volumes. Experiments marked by turbulent flow are not reported.

4.2. *Observations*

4.2.1. *Bubble shapes*. Figure 6 illustrates qualitatively the dependence of the bubble shape and stability on the bubble Reynolds number and Eotvos number, observed in our experiments, for air bubbles rising through distilled water. The progression of shapes with increasing bubble volume is similar to that reported by Siekmann *et al*. (1974). Bubble forms include stable circular bubbles, wobbling oblate ellipses (characterized by periodic vortex shedding in their wakes), unstable oblate ellipses, stable circular caps, and unstable circular caps. We focus on the parameter regime in which stable bubbles and accompanying stable wakes obtain; specifically, stable elliptical caps and stable oblate ellipses. In these cases, the compound body comprised of bubble plus wake was roughly elliptical, in accordance with the observations of Collins (1965a) and Lazarek and Littman (1974).

4.2.2. *Adjustment phase*. In figure 7, we present a series of photographs depicting the adjustment phase which follows a volume of air being injected at the lower boundary. The initial volume of injected air is roughly circular, but adjusts to a circular cap shape over a distance of

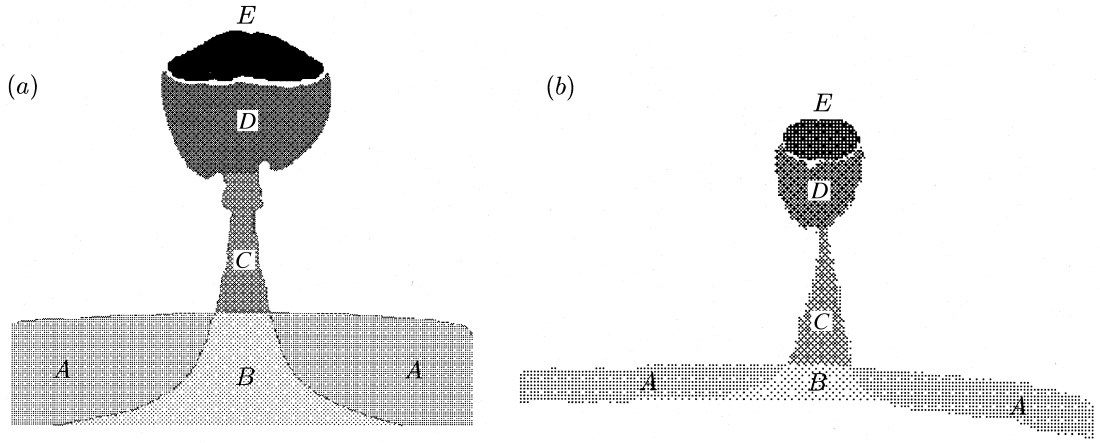

Figure 5. Post-processed images illustrating the distortion of an originally horizontal milk–water interface by the motion of (a) a circular cap bubble, and (b) an oblate elliptical bubble. The bubbles are denoted by (E) and their primary wakes by (D). In each case, the areas between the original and final interface locations yield the drift volume (B + C) and the reflux volume (A + B). The images span the full channel width.

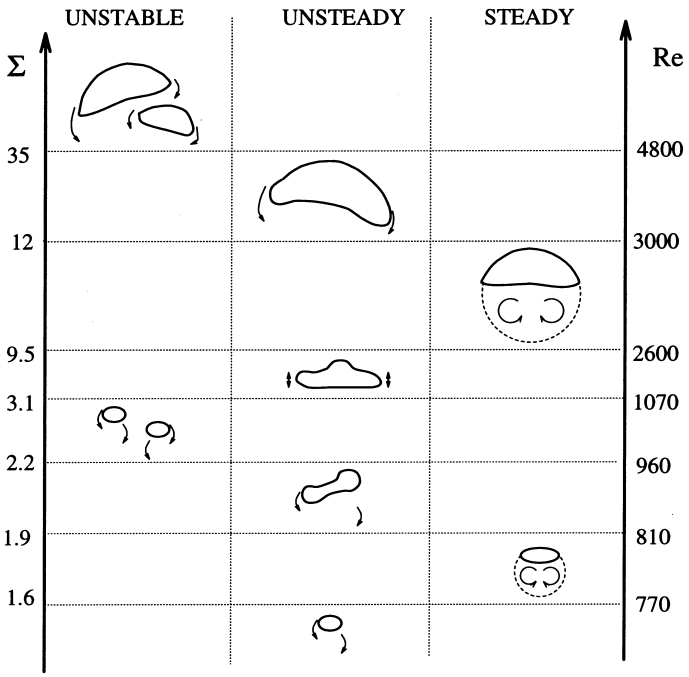

Figure 6. The observed shape and form of motion of air bubbles rising through a thin gap of water, where the gap thickness was 0.25 cm and the inclination angle $\theta = 15°$. The Reynolds and Eotvos numbers, respectively, $Re = Ur/\nu$ and $\Sigma = \rho r^2 g \sin\theta/\sigma$ are based on the undeformed bubble radius r. For certain parameter ranges the bubbles were unstable and broke. In others, the bubble motion was unsteady, and characterized by either periodic or aperiodic oscillations. The parameter regime of interest in our study of fluid transport is that characterized by the steady rectilinear motion of stable bubbles.

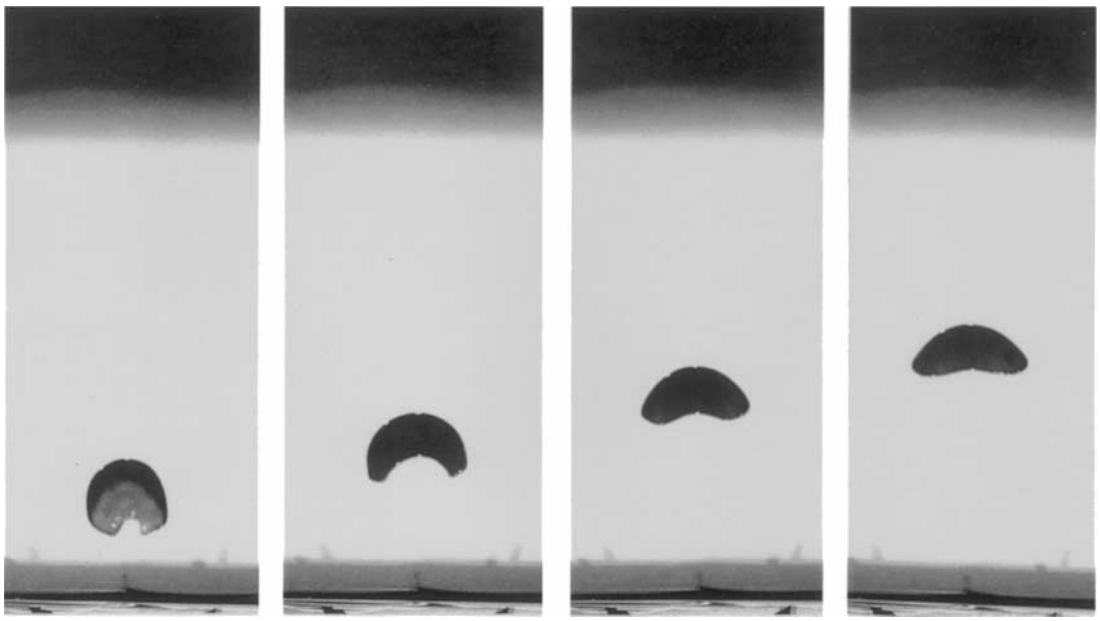

Figure 7. A sequence of photographs of an initially nearly circular air bubble injected at the lower boundary rising towards a milk–water interface and adjusting to a circular cap form. The time between consecutive photographs is 1/3 seconds. The adjustment process is characterized by the deformation of the bubble to a steady shape and its acceleration to a steady rise speed, and is complete after the bubble has risen a distance comparable to $4a$, where a is the half-width of the bubble in its final form. Note that the bubble width increases during the adjustment process. Only a fraction of the channel width is shown.

approximately four bubble radii. The adjustment sequence is qualitatively similar to that observed by Walters and Davidson (1962) for initially circular air bubbles released in a narrow gap of water. After the adjustment phase, the bubble achieves a steady rise speed $U \sim 0.42(ag \sin\theta)^{1/2}$ whose dependence on the ratio of the bubble width to channel width was found to be consistent with the experimental observations and theoretical predictions of Collins (1965b).

4.2.3. *Particle trajectories.* Figure 8 is an example of the data obtained from particle tracking, and illustrates the displacement of particles by the flow accompanying a rising bubble. In the particle tracking experiments, the entirety of the fluid motion was followed, so the contribution to fluid displacement from the secondary wake was evident. For the sake of comparison, we include the trajectories predicted on the basis of the theory described in Section 3.3. The area examined in this experiment was more than a channel width from the point of injection. The particle displacements were observed to be largely independent of z in accordance with theory; consequently, the approximate form of the distortion of any material surface within the tracked region may be calculated by collapsing all of the starting points of the observed particle trajectories down onto a single line, denoted in figure 8 as $z = 0$. Figure 8 indicates a roughly uniform reflux, as well as a typically poorly resolved drift profile. Far from the centerline, the displacement is almost entirely vertical and corresponds roughly to a uniform reflux. Close to the centerline, particles pass close to the stagnation point on the nose of the bubble, and so are displaced a significant distance forward. The breaking of fore–aft symmetry in the particle trajectories near the centerline was also observed by Weber and Bhaga (1982), and is a manifestation of the presence of the secondary wake trailing the bubble. We note that the influence of the secondary wake was not as pronounced in the interface tracking experiments, since we there

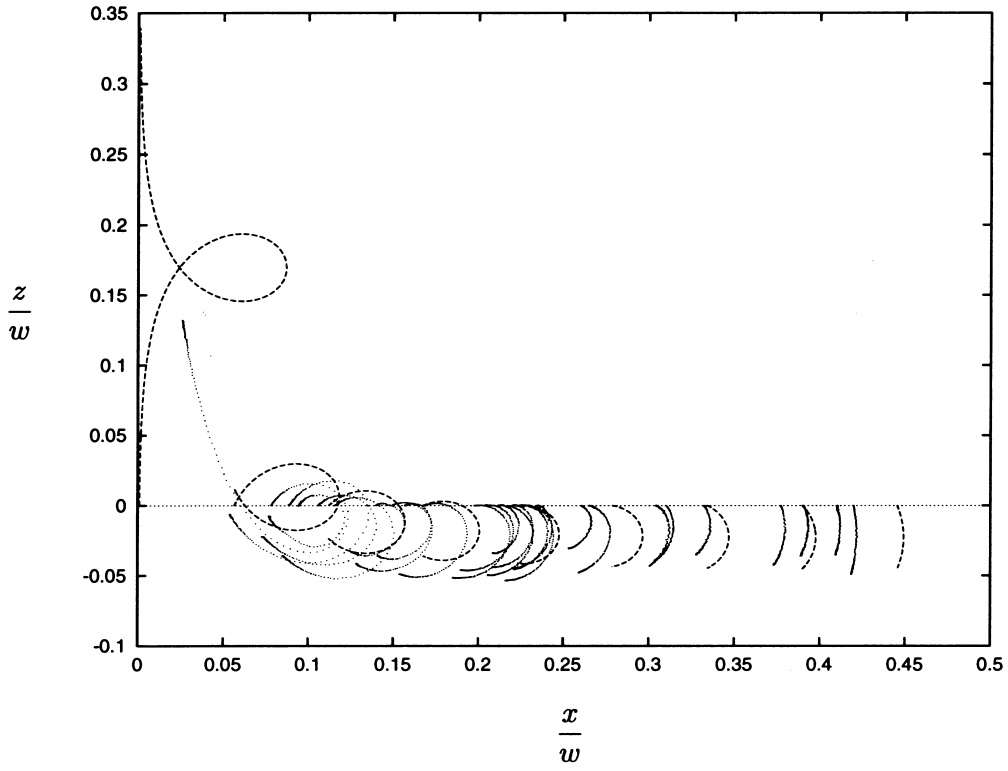

Figure 8. Observed trajectories of neutrally buoyant plyolite particles suspended in a saltwater solution. An elliptical cap bubble with half-width $a = 3.5$ cm was injected and subsequently rose along the centerline ($x = 0$) of a channel 40 cm in width. The height to width ratio of the compound body was 8/7. Particles starting within a 40 cm by 40 cm area a distance 30 cm from the lower boundary were tracked. In processing the data, the initial vertical position of the particles were shifted so that each trajectory began from a single horizontal line, here denoted by $z = 0$. For comparison, the trajectories (dashed lines) predicted to arise as a circular cylinder (with the same width as the bubble) rises along the channel are included.

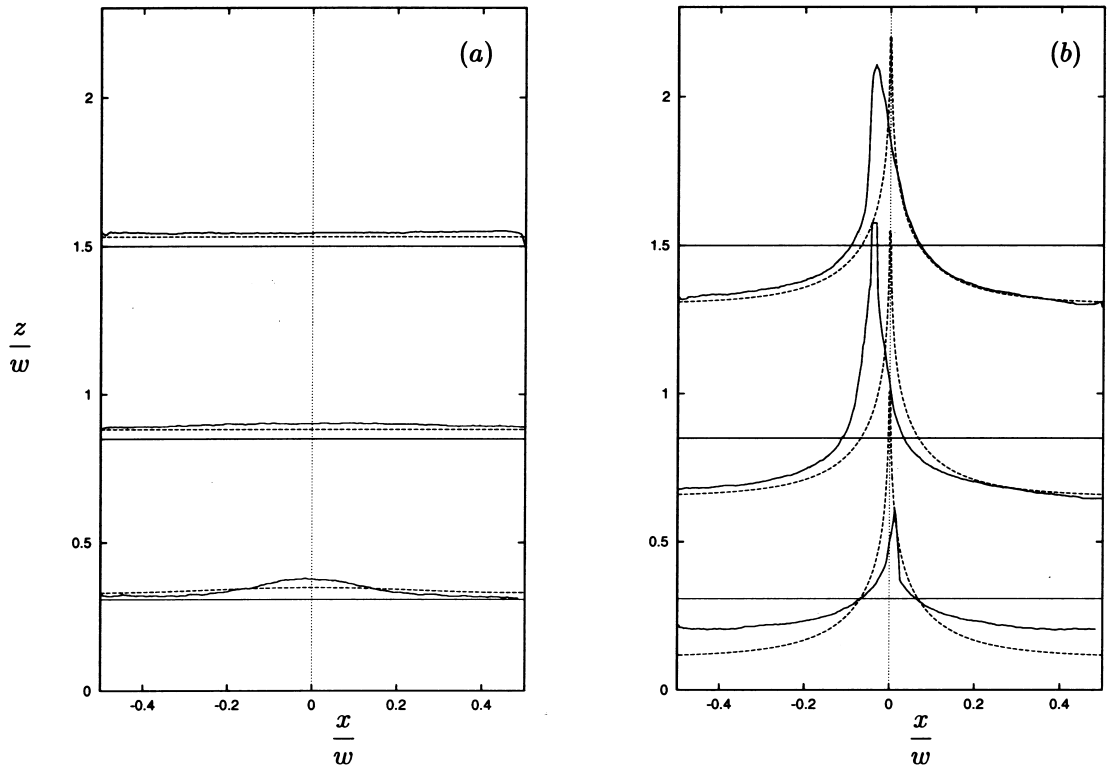

Figure 9. The observed distortion profiles at three levels associated with the injection and subsequent translation of a circular cap bubble with a circular compound body of radius 3.8 cm rising in a channel of width $w = 20$ cm. The observed (solid) and theoretically predicted (dashed) injection-induced distortions are presented in (*a*), while the final interface shapes are given in (*b*).

examined the distortion profiles after the bubble had risen a distance comparable to the channel width.

4.2.4. *Distortion profiles*. Figure 9(a) illustrates the injection-induced distortion profiles of three initially horizontal interfaces at different distances from the lower boundary. The theoretically predicted distortion profiles are included for comparison. The observations confirm that the injection-induced distortion is non-uniform in the vicinity of the lower boundary, but is uniform at distances comparable to the channel width. The small discrepancy in amplitude for the upper two interfaces indicates the typical reading errors in our experiments, which were introduced by the interface not being perpendicular to the channel walls (see Section 4.3). The theory reported in Section 3.1 assumes that the amplitude of the injection-induced displacement is much smaller than the initial distance between the point of injection and the interface, and it is this limitation of the theoretical model which accounts for the marked discrepancy between the experiments and theory for the lowermost profile.

Figure 9(b) illustrates the permanent distortion to three initially horizontal interfaces by the injection and subsequent translation of a circular cap bubble with a stable primary wake. In accordance with the potential flow model, the distortion profiles are characterised by a localized drift and a distributed uniform reflux. The interface shape predicted to exist far from the lower boundary $z \gg w$, obtained by superposing the unbounded drift profile on the appropriate uniform reflux, is included for the sake of comparison. This far-field distortion profile approximately matches the upper two interfaces, both of which are initially at distances greater than half the channel width from the lower boundary. The lower interface takes a final form which is markedly different, owing to the proximity of the lower boundary and the complicated time-dependent nature of the injection and adjustment phases in the laboratory flow. In particular, the bubble is still adjusting towards its equilibrium shape as it passes through the interface, and its primary wake has yet to develop fully.

Table 1. The parameter regime examined in the experimental study

θ	Re	$Re(d/a)^2$	$2a/w$	$w/2z$	a/z	ϵ	C_m'
10°–15°	1000–6500	11–54	0.1–0.6	0.4–2.2	0.1–0.65	1.5–4	0.7–1.4

4.2.5. *Drift volume*. Table 1 summarizes the parameter regime explored in our interface tracking studies. Within this parameter regime, the bubbles observed were either oblate or elliptical caps, the primary wake varied in shape such that ϵ varied from 1.5 to 4, rise speeds U varied between 5.7 and 11.9 cm/s, bubble half-widths a between 0.8 and 8.8 cm, channel widths w between 12 and 41 cm, and the added mass coefficient $C_m' = a/b$ between 0.7 to 1.4. The flow within the channel was laminar, and we ensured that criterion [5] was satisfied everywhere, so that viscous interaction with the channel walls did not significantly impact the flow.

Figure 10 illustrates the dependence of the ratio of the drift volume to πa^2 on the normalized distance z/a from the point of injection (the lower boundary) to the material surface (milk–water interface). According to the potential flow description, [13], this ratio should approach unity at sufficient distance from the lower boundary. For $z/a > 0.4$, the observed drift volumes are in accord with the potential flow model, which predicts that the drift volume depends only on the width of the rising compound body. The errors in the reported drift volumes are discussed in Section 4.3. For $z/a < 0.4$, the inviscid flow model overpredicts the drift volume. This discrepancy is associated with the fact that the bubble is still adjusting, and its wake developing, as it passes through the interface; consequently, the radius of the compound body as it passes through the interface is significantly less than that measured once a steady state has been established.

4.3. *Discussion of errors*

In our experimental study, we were constrained to consider a limited range of Reynolds numbers. Below a critical value, defined by [5], the influence of the channel walls became significant

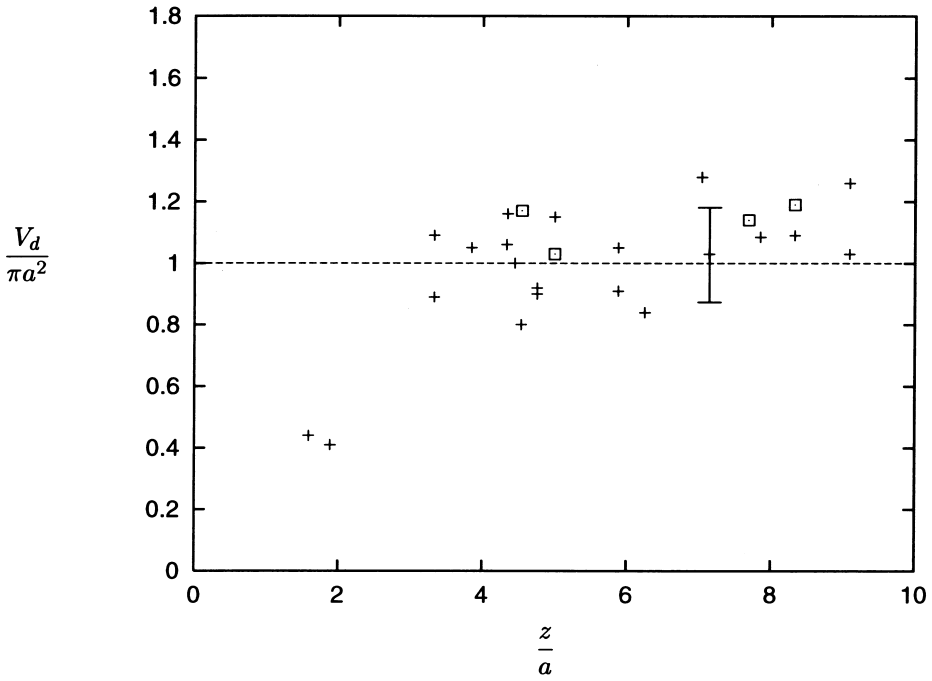

Figure 10. The variation of measured drift volumes with distance between the point of injection and the material surface considered. + denote circular cap bubbles, and □ oblate elliptical bubbles. The dashed line corresponds to the result anticipated in an unbounded channel on the basis of inviscid flow theory, namely, that the ratio of the drift to compound body volumes should be precisely equal to the added mass coefficient of the compound body.

so that the bulk flow within the channel could not be adequately described by two-dimensional inviscid flow theory. Above a critical value, boundary layer instability gave rise to turbulent flow within the channel. For a bubble of a given volume, the desired high Reynolds number laminar flow could be achieved only in a limited range of tank inclinations. For the bubble sizes considered in our study, $1\text{ cm} < a < 5\text{ cm}$, it was necessary to operate in the regime $10^\circ < \theta < 15^\circ$. Such low inclination angles introduced a number of three-dimensional flow effects which were the principal sources of error in our experiments.

The principal difficulty associated with the particle tracking arose from the particle-wall interactions. This was particularly evident upstream of the bubble, where particles occasionally stuck to the glass walls, and were only dislodged by direct collision with the bubble. This problem could not be eliminated entirely, but was alleviated by ensuring that the particles were neutrally buoyant. The shallow inclination angles also prevented the flow from being symmetric about the mid-plane of the channel, so that in the interface tracking experiments, the milk–water interface was not perpendicular to the channel walls. This leads to an error in identifying the position of the interface, and in turn to an error of roughly 15% in the reported drift volumes.

Secondary sources of error in the interface studies include the uncertainty in distinguishing between the primary wake and drift volumes, slight changes in bubble shape as the bubble crossed the interface, and weak time-dependence of the volume and shape of the primary wake.

Finally, it is worth noting that it was difficult to determine to what extent the secondary wake contributed to the observed fluid transport. By measuring the distortion profiles after a finite time (corresponding to the time over which the fluid displacement associated with the potential flow is complete), we attempted to minimize the contribution to fluid transport made by the secondary wake. The subsequent distortion, influenced by both the secondary wake and the weak density change across the interface, was both weak and short-lived, and contributed no more than an additional 15% to the reported drift volumes.

The presence of impurities in the water may act to rigidify bubble surfaces, thus generating vorticity at the bubble surface (Hartunian and Sears 1957) and so intensifying the secondary wake. Moreover, the detailed boundary layer structure may be quite complex in this thin-gap geometry owing to the interaction between the bubble surface and the channel walls. In particular, Bush (1997) has identified an unusual wake structure accompanying bubble motion in a thin gap at low gap Reynolds numbers which is associated with the mechanical redistribution of surfactant material by the rolling bubble surface.

5. MIXING BY BUBBLES

On the basis of our physical picture of the irrotational fluid displacement accompanying individual bubbles, we proceed by describing a simple heuristic model of mixing by an assemblage of high *Re* bubbles. The model is simplified in that the fluid transport in the secondary wake is neglected, and bubble–bubble interactions are assumed to be negligible. This model of bubble-induced mixing represents a straightforward application of the more general model of mixing by obstacles in potential flow developed by Eames and Bush (1998).

Consider a tank of fluid which initially consists of two superposed layers of fluid, the upper layer being clear and the lower layer dyed. Bubbles are released continuously from inlets distributed along the lower boundary. We are concerned with describing the evolution of the interface which is disrupted by the rising bubbles. We assume that the bubble motion has the form described in this paper: bubbles of volume V rise at a uniform speed U accompanied by stable primary wakes of volume ϵV, and drift volumes $C_{\mathrm{m}}{}'V(1+\epsilon)$. As the bubbles pass through the interface, the fluid transport will be characterized by a localized drift near the points of crossing and a broad reflux across the channel width. The volume fraction α of bubbles is assumed to be sufficiently small that bubble–bubble interactions may be neglected. Individual bubbles are influenced only by the reflux associated with their neighbours, and so rise at a hindered speed $U_h = U(1-\alpha(1+\epsilon)C_{\mathrm{m}}{}')$.

The interface will drop relative to the container walls at an average rate $\bar{u} = \alpha\epsilon U$ in response to the dyed fluid being transported to the surface of the container in the primary wake. In the

absence of molecular diffusivity, the erosion of the interface may be characterized entirely by a bubble-induced mechanical dispersion coefficient D_L. On dimensional grounds, we expect D_L to be proportional to the volume fraction of the compound bodies $\alpha(1 + \epsilon)$, the bubble rise speed U_h, and the lengthscale L characteristic of the longitudinal displacement, specifically, the center of mass of the drift volume. A formal treatment demonstrates that the appropriate constant of proportionality is the added mass coefficient of the compound body, C_{m}', so that the dispersion coefficient may be expressed in general by $D_L = C_{\mathrm{m}}'(1 + \epsilon)\alpha U_h L$ (Eames and Bush, 1998).

In the neighbourhood of the interface, the horizontally averaged concentration of the lower fluid $C(z,t)$ thus satisfies an advection–diffusion equation of the form

$$\frac{\partial C}{\partial t} = -\bar{u}\frac{\partial C}{\partial z} + D_L\frac{\partial^2 C}{\partial z^2} \qquad [18]$$

The evolution of the system is thus governed solely by the volume fraction of bubbles α as well as ϵ and C_{m}', which are uniquely prescribed by the bubble parameters, Re and Σ. The presence of a primary wake does not significantly alter the width of the compound body (Bhaga and Weber, 1981), and so does not effect the drift volume. Nonetheless, the primary wake does have two significant effects on the efficiency of fluid transport: firstly, it advects fluid with the bubble, thus generating an enhanced reflux; secondly, it changes the added mass coefficient of the compound body, and so promotes heightened longitudinal dispersion.

It is important to realize that in three dimensions, the secondary wake will be more pronounced than in our two-dimensional experiments and will make a significant contribution to the fluid transported by the bubbles. Consequently, our simple model based on the irrotational component of the flow will underpredict the efficiency of bubble-induced mixing, and the expression given for the mechanical dispersion coefficient represents a lower bound.

6. CONCLUSION

We have presented an experimental study of two-phase flow in which we examined the fluid displacement associated with high Reynolds number bubble motion in a thin gap. We specifically chose to undertake a two-dimensional experimental study, because the effects of drift and reflux are more pronounced in two dimensions. In particular, the drift profile drops off from the centerline as $1/x^3$ in two dimensions and as $1/x^5$ in three dimensions, and the reflux amplitude scales with container width R as $1/R$ in two dimensions rather than $1/R^2$ in three. Moreover, the two-dimensional channel geometry tremendously simplified the flow visualization, and made it possible to consider the desired parameter regime of large bubbles with stable primary wakes.

The parameter regime considered in the experiments was that characterized by high Reynolds number laminar flow, in which wall effects were negligible to leading order. Nevertheless, viscous effects were evident in the experimental study, and contributed to fluid transport in the secondary wake trailing the bubble. The influence of the secondary wake was apparent in the particle tracking experiments, and was made manifest by fore–aft asymmetry in the particle trajectories. Owing to the damping influence of the channel walls, it was not deemed valuable to quantify the fluid transport in the secondary wake. Consequently, in the interface tracking studies, the distortion profiles were measured after the bubble had risen a distance comparable to the channel width, by which time the potential flow contribution to the fluid displacement had been made. The subsequent distortion, associated with the secondary wake trailing the bubble, was both weak and short-lived, and did not make a substantial contribution to the net fluid transport.

The experiments were directed towards quantifying the form of the fluid displacement associated with the injection and subsequent translation of single bubbles in a two-dimensional channel. The two-dimensional inviscid flow model describes to leading order the bubble-induced distortion of a material surface, as well as the measured drift and reflux volumes. The theory predicts that, within half the channel width of the lower boundary, both the injection-induced distortion and reflux are non-uniform across the channel. While this prediction was confirmed by our experimental observations, quantitative agreement between observed and predicted dis-

tortion profiles in the vicinity of the lower boundary was not possible owing to the complicated adjustment process which followed the bubble injection, and the influence of the lower boundary. In general, the drift volume in regions close to the lower boundary was less than that in the far field, since the cross-sectional area of the bubble increases during the adjustment period.

Quantitative agreement between the theory and experiments was obtained at distances greater than half the channel width from the point of injection. In this far-field region, the drift volume does not depend on the bounding geometry; moreover, it is not simply related to the bubble volume, but rather to the cross-sectional area of the compound body presented to the flow. The drift volume depends on the details of the primary wake only insofar as it may change the exposed area of the compound body. The final shape of the distortion profile does, however, depend explicitly on the shape of the compound body, with its peak being more pronounced for more oblate bodies. Furthermore, we have demonstrated that, in the far-field, the fluid reflux is uniform across the channel width, and has an amplitude which depends critically on the volume of the primary wake, the drift volume and the channel width.

We have demonstrated that a substantial component of the fluid transport associated with bubbles with stable primary wakes may be deduced by treating the induced flow as potential flow around the compound body composed of bubble plus wake. Although we have focussed on a two-dimensional geometry, many of our conclusions carry over to the three-dimensional problem. In three dimensions, stable rectilinear motion of bubbles with or without stable primary wakes is observed in the range $50 < Re < 500$, which describes air bubbles with diameter 0.1–1.2 mm rising through water (Clift *et al.* 1978). As the Reynolds number increases through this range, bubbles become progressively more oblate (Moore 1965). The added mass coefficient of an ellipsoidal body with semi-major and -minor axes of, respectively, a and b is given exactly by

$$C_{\mathrm{m}} = \frac{\alpha_0}{2-\alpha_0}, \text{ where } \alpha_0 = a^2 b \int_0^\infty \frac{\mathrm{d}\lambda}{(\lambda + a^2)^{\frac{3}{2}}(\lambda^2 + b^2)}, \qquad [19]$$

(Lamb 1932), which in the limit of large oblate distortions, $a/b \gg 1$, takes the form

$$C_{\mathrm{m}} \sim \frac{2}{\pi}\frac{a}{b}. \qquad [20]$$

In this asymptotic limit, the drift volume $V_{\mathrm{d}} = C_{\mathrm{m}} \frac{4}{3}\pi a^2 b = \frac{8}{3}a^3$ is once again uniquely determined by the cross-sectional area of the bubble. We note that typically C_m may be significantly different from the value of 0.5 assumed in a number of theoretical models (Kowe *et al.* 1988). As in the two-dimensional case, the drift volume is uniquely prescribed by the shape of the compound body, which is in turn prescribed by Re and Σ. Finally, on the basis of our theoretical model, it should be straightforward to encorporate the extensive data compiled on the form of bubbles and wakes in three-dimensions (Clift *et al.*, 1978; Bhaga and Weber 1981) in order to predict the drift volumes associated with high Reynolds number bubble motion in three dimensions.

It is important to emphasize that the velocity field in the secondary wake trailing a three-dimensional bubble drops off much more slowly than the potential flow component with distance from the bubble; consequently, the transport in the secondary wake may also contribute substantially to observed drift volumes and thus to reflux amplitudes. When $Re \sim 50$, the hydrodynamic drag on a spherical air bubble of radius a rising through water is $D = 6\pi\rho\nu Ua$; consequently, according to [1], the volume flux in the secondary wake is $Q = 6\pi\nu a$ far downstream. When the flow around the bubble separates, so that a primary wake region exists, the drag increases by a factor of $O(Re)$, as must the associated volume flux in the far-field secondary wake. Consequently, while the presence of the primary wake does not significantly alter the contribution to the fluid displacement made by the potential flow (drift) component, it does indicate that the contribution from the secondary wake will be more significant. The importance of the transport in the secondary wake, and its dependence on the form of the translating body (either a bubble, a fluid drop or a rigid particle) and on the bounding geometry, will be the subject of future research.

Acknowledgements—JWMB gratefully acknowledges the financial support of an NSERC of Canada post-doctoral fellowship. IE acknowledges the support through the Jeremy Howarth Fellowship at St. Catharine's College. The authors thank Stuart Dalziel for numerous helpful suggestions concerning the experiments, and Paul Linden for his generously granting us access to the DAMTP laboratory facilities.

REFERENCES

Asaeda, T. and Imberger, J. (1993) Structure of bubble plumes in linearly stratified environments. *J. Fluid Mech.* **249,** 35–57.

Bataille, J., Lance, M. and Marie, J. L. (1991) Some Aspects of the Modeling of Bubbly Flows. In *Phase-Interface Phenomena in Multiphase Flow*, ed. G.F., Hewitt, F., Mayinger, J.R., Riznic, pp. 179–193.

Batchelor, G. K. (1967) *An introduction to fluid dynamics*. Cambridge University Press.

Bessler, W. F. and Littman, H. (1987) Experimental studies of wakes behind circularly capped bubbles. *J. Fluid Mech.* **185,** 137–151.

Bhaga, D. and Weber, M. E. (1981) Bubbles in viscous liquids: shapes, wakes and velocities. *J. Fluid Mech.* **105,** 61–85.

Bush, J. W. M. (1997) The anomalous wake accompanying bubbles rising in a thin gap: a mechanically forced Marangoni flow. *J. Fluid Mech.* **352**, 283–303.

Clift, R., Grace, J. R. and Weber, M. E. (1978) *Bubbles, Drops and Particles*. Academic Press.

Collins, R. (1965a) Structure and behaviour of wakes behind two-dimensional air bubbles in water. *Chem. Eng. Sci.* **20,** 851–853.

Collins, R. (1965b) A simple model of the plane gas bubble in a finite fluid. *J. Fluid Mech.* **22,** 763–771.

Dalziel, S. B. (1992) Decay of rotating turbulence: some particle tracking experiments. *Applied scientific research* **49,** 217–244.

Darwin, C. (1953) A note on hydrodynamics. *Proc. Cam. Phil. Soc.* **49,** 342–354.

Davidson, T. and Harrison, D. (1963) *Fluidised particles*. Cambridge University Press.

Davies, R. M. and Taylor, G. I. (1950) The mechanics of large bubbles rising through extended liquids and through liquids in tubes. *Proc. Roy. Soc. A* **200,** 375–390.

Duineveld, P. C. (1995) The rise velocity and shape of bubbles in pure water at high Reynolds number. *J. Fluid Mech.* **292,** 325–332.

Eames, I. and Bush, J. W. M. (1998) Longitudinal dispersion by bodies fixed in a potential flow, submitted to *J. Fluid Mech.*

Eames, I., Belcher, S. E. and Hunt, J. C. R. (1994) Drift, partial drift and Darwin's proposition. *J. Fluid Mech.* **275,** 201–223.

Eames, I. and Duursma, G. R. (1997) Displacement of horizontal layers by bubbles injected into fluidised beds, *Chem. Eng. Sci.*, **52,** 2697–2705.

Hartunian, R. A. and Sears, W. R. (1957) On the instability of small gas bubbles moving uniformly in various liquids. *J. Fluid Mech.* **3,** 27–47.

Kowe, R., Hunt, J. C. R., Hunt, A., Couet, B. and Bradbury, L. J. S. (1988) The effects of bubbles on the volume fluxes and the pressure gradients in unsteady and non-uniform flow of liquids. *Int. J. Multiphase Flow* **14,** 587–606.

Lamb, H. (1932) *Hydrodynamics*. Cambridge University Press.

Lazarek, G. M. and Littman, H. (1974) The pressure field due to a large circular capped air bubble rising in water. *J. Fluid Mech.* **66,** 673–687.

Maxworthy, T. (1967) A note on the existence of wakes behind large, rising bubbles. *J. Fluid Mech.* **27,** 367–368.

Maxworthy, T., Gnann, C., Kurten, M. and Durst, F. (1996) Experiments on the rise of air bubbles in clean viscous fluids. *J. Fluid Mech.* **321,** 421–441.

Mayinger, F., Chen, Y. M. and Nordmann, D. (1992) Heat transfer at the phase-interface of conducting bubbles. In *Phase-Interface Phenomena in Multiphase Flow*, ed. G.F. Hewitt, F. Mayinger and J.R. Riznic, pp. 433–442.

Moore, D. W. (1965) The velocity of rise of distorted gas bubbles in a liquid of small viscosity. *J. Fluid Mech.* **23,** 749–765.

Ryskin, G. and Leal, L. G. (1984) Numerical solution of free-boundary problems in fluid mechanics. Part 2. Buoyancy-driven motion of a gas bubble through a quiescent liquid. *J. Fluid Mech.* **148,** 19–35.

Saffman, P. G. (1956) On the rise of small air bubbles in water. *J. Fluid Mech.* **1,** 249–275.

Siekmann, J., Eck, W. and Johann, W. (1974) Experimentelle Untersuchungen uber das Verhalten von Gasblasen in einem Null-g-Simulator. *Z. Flugwiss.* **22,** 83–92.

Walters, J. K. and Davidson, J. F. (1962) The initial motion of a gas bubble formed in an inviscid liquid, Part 1. The two-dimensional bubble. *J. Fluid Mech.* **12,** 408–416.

Weber, M. E. and Bhaga, D. (1982) Fluid drift by a rising bubble. *Chem. Eng. Sci.* **37,** 113–116.